

Fe₂Mo₃O₈ nanoparticles self-assembling 3D mesoporous hollow spheres toward superior lithium storage properties

Lifeng Zhang (✉)^{1,2}, Yifei Song¹, Weiping Wu (✉)², Robert Bradley^{3,4,5}, Yue Hu¹, Yi Liu¹, Shouwu Guo (✉)^{1,6}

¹ School of Materials Science and Engineering, Shaanxi University of Science and Technology, Xi'an 710021, China

² Department of Electrical and Electronic Engineering, School of Mathematics, Computer Science and Engineering, City, University of London, London, EC1V 0HB, UK

³ Department of Materials, University of Oxford, Oxford, OX1 3PH, UK

⁴ MatSurf Technology Ltd., The Old Stables Marion Lodge, Cumbria, CA10 1NW, UK

⁵ School of Energy Resources, University of Wyoming, Laramie, WY 82071, USA

⁶ School of Electronic Information and Electrical Engineering, Shanghai Jiao Tong University, Shanghai 200240, China

© Higher Education Press 2020

Abstract Unique self-assembled iron(II) molybdenum (IV) oxide (Fe₂Mo₃O₈) mesoporous hollow spheres have been facilely constructed *via* the bubble-template-assisted hydrothermal synthesis method combined with simple calcination. The compact assembly of small nanoparticles on the surface of the hollow spheres not only provides more active sites for the Fe₂Mo₃O₈, but also benefits the stability of the hollow structure, and thus improved the lithium storage properties of Fe₂Mo₃O₈. The Fe₂Mo₃O₈ mesoporous hollow spheres exhibit high initial discharge and charge capacities of 1189 and 997 mA·h·g⁻¹ respectively, as well as good long-term cycling stability (866 mA·h·g⁻¹ over 70 cycles) when used as a lithium-ion battery anode. This feasible material synthesis strategy will inspire the variation of structural design in other ternary metal molybdates.

Keywords molybdates, Fe₂Mo₃O₈, hollow spheres, lithium ion batteries, anodes

1 Introduction

Ternary metal molybdates (M₂Mo₃O₈) are an emerging class of important inorganic functional materials which are widely used in various fields such as electromagnetic response, corrosion inhibitors, photoelectric catalysis [1–3]. In recent years, with the rapid development of high energy density lithium ion batteries, transition

metal molybdates and tungstates (M₂Mo₃O₈, M₂W₃O₈ and so on) have attracted much attention as ideal candidates to substitute for the traditional graphite anode materials, due to their high theoretical capacity, low cost and structural diversity [4]. Although various M₂Mo₃O₈ (M: Co, Mn, Zn, Fe) have been synthesized and tested as Lithium ion batteries anodes, their unfavorable microstructures such as high density, aggregated particles or platelets inevitably resulted in inferior capability and cyclability [5–11]. Synthesis of hollow sphere structures of carbon and inorganic materials have been an effective strategy to tackle the above challenges [12–15]. The hollow structures with large specific surface area and high porosity, can not only provide more active sites, but also shorten the Li⁺ diffusion lengths. Furthermore, the porous hollow structure is also benefited to facilitate electrolyte penetration, thus providing more interface area between electrode material and electrolyte [16–19]. However, the M₂Mo₃O₈ with hollow sphere structures are rarely reported [20], due to the complexity and aggregation of their microstructures.

The bubble-template-assisted hydrothermal synthesis method is a unique and interesting synthesis method for the construction of hollow metal oxide/sulfide spheres. Since Eschenauer' group proposed the concept of bubble iterative positioning in 1994 [21], many hollow metal oxide/sulfide structures such as NiO, CoO, MoS₂ [22–25] have been synthesized and studied as lithium ion battery electrodes. Herein, we applied the bubble-template-assisted hydrothermal synthesis method and combined it with calcination to produce the Fe₂Mo₃O₈ mesoporous hollow spheres and improved their lithium storage properties. The obtained Fe₂Mo₃O₈ material have the unique hollow sphere architecture with a wall thickness of about

Received March 7, 2020; accepted July 6, 2020

E-mails: zhanglifeng@sust.edu.cn (Zhang L F);

Weiping.Wu@city.ac.uk (Wu W P);

guoshouwu@outlook.com (Guo S W)

100 nm. When evaluated as a lithium ion battery anode, the Fe₂Mo₃O₈ hollow spheres deliver a high reversible capacity and improved cycling capability. The well-constructed morphology and superior electrochemical performance of Fe₂Mo₃O₈ hollow spheres, indicated that the method is a new approach towards the synthesis of other molybdate and tungstate based hollow spheres with low cost and high performance.

2 Experimental

2.1 Materials synthesis

Iron(III) nitrate 9-hydrate (Fe(NO₃)₃·9H₂O, 1.077 g) was dissolved in the mixed solution of 36 mL ethylene glycol and 4 mL nitric acid. Ammonium molybdate tetrahydrate ((NH₄)₆Mo₇O₂₄·4H₂O, 0.706 g) was dissolved in 40 mL ethylene glycol. Then the iron nitrate solution was added dropwise into ammonium molybdate solution under magnetic stirring in 30 min. The mixture was then transferred into a 100 mL Teflon lined stainless steel autoclave and heated at 160 °C for 12 h. After the reaction and cooling, the product was collected by centrifugation and dried at 60 °C for 12 h. Then the powder was annealed in Ar atmosphere at 500 °C for 2 h with a heating rate of 5 °C·min⁻¹.

2.2 Material characterizations

The morphologies of materials were characterized by field emission scanning electron microscope (FESEM, Hitachi S-4800) and transmission electron microscopy (TEM, FEI Tecnai G2 F20). The X-ray diffraction (XRD, Rigaku, D/max-2200 PC) patterns were acquired on a Rigaku Ultima IV X-ray diffractometer with Cu K α ($\lambda = 1.54178 \text{ \AA}$) radiation. The X-ray photoelectron spectroscopy (XPS) was performed with a ULVAC-PHI5000 spectrometer with Al K α radiation. The Brunauer-Emmett-Teller (BET) surface area was determined by the nitrogen adsorption isotherm at 77 K using a Micromeritics ASAP 2460 surface area and porosity analyzer.

2.3 Electrochemical measurements

The electrochemical properties were evaluated using coin cells (CR2032) assembled in an Ar filled glove box with lithium foil as a counter electrode. The working electrodes were prepared by mixing the active material (Fe₂Mo₃O₈) with acetylene black and polyvinylidene fluoride in a weight ratio of 8:1:1 in *N*-methyl-2-pyrrolidone. The slurry was then coated on the copper foil and dried at 110 °C for 12 h under vacuum. The Celgard 2500 polypropylene film and 1 mol·L⁻¹ lithium hexafluorophosphate (LiPF₆) in ethylene carbonate and dimethyl carbonate (1:1 in volume) were used as a separator and the electrolyte, respectively. Cyclic voltammetry (CV) was performed on a CHI 660E electrochemical workstation. The galvanostatic charge-discharge tests were performed using a Newaresles battery test system (Shenzhen, China) with a cutoff voltage of 3.00–0.01 V vs. Li/Li⁺ at room temperature. The electrochemical impedance spectral measurements were carried out in the frequency range from 100 kHz to 0.01 Hz.

3 Results and discussion

Figure 1 illustrates the schematic procedures for the general synthesis of Fe₂Mo₃O₈ hollow spheres. Under the solvothermal condition, ethylene glycol reduces Fe³⁺ to Fe²⁺ and synchronously released bubbles of low boiling oxidation products such as acetaldehyde and glycolaldehyde etc. [26,27]. In order to reduce surface free energy, the Fe²⁺ and MoO₄²⁻ ions concentrated on the surface of bubble templates and nucleated to form iron(II) molybdate FeMoO₄ [28,29]. Then, the FeMoO₄ nuclei were aggregated together forming the initial shell, whose morphology and phase structure were shown in Fig. S1 (cf. Electronic Supplementary Material, ESM). After calcination under Ar at 500 °C for 2 h, the spherical shell was preserved, while the FeMoO₄ phase was converted to Fe₂Mo₃O₈ due to the phase transition of the crystals. Consequently, three dimensions (3D) Fe₂Mo₃O₈ hollow spheres self-assembled by the small nanoparticles were formed.

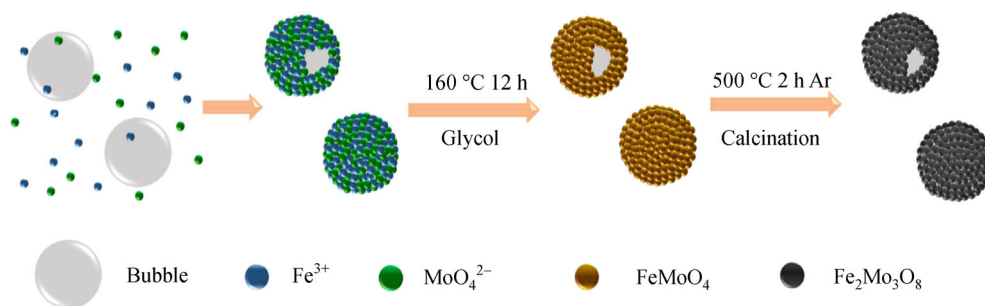


Fig. 1 Schematic illustration of the general synthesis strategy for Fe₂Mo₃O₈ hollow spheres.

Figure 2(a) shows a typical FESEM image of the as-synthesized $\text{Fe}_2\text{Mo}_3\text{O}_8$ hollow spheres. Spherical morphology with a rough surface and diameter in the range of 0.7–1.2 μm can be clearly seen. Some aggregated nanoparticles appear near the hollow spheres as well as the precursors (Fig. 2(a), Fig. S1), which may be due to the immature growth of crystals during the formation of hollow spheres. Figure 2(b) shows the magnified SEM image of the crack edge of hollow spheres. Particles ranging in size from 10 to 20 nm were observed on the surface of the spheres. Figures 2(c) and 2(d) are the TEM and high resolution TEM (HRTEM) images of as-synthesized $\text{Fe}_2\text{Mo}_3\text{O}_8$, respectively. The hollow sphere structure is distinctly identified, the TEM images also confirmed the average shell thickness is 120 ± 10 nm (Fig. 2(c)). The HRTEM image reveals the interplanar distance of the lattice fringes of 0.25 nm, corresponding to the (112) crystal planes of $\text{Fe}_2\text{Mo}_3\text{O}_8$ (Fig. 2(d)).

The XRD characterizations further determined the crystallographic structures of the as-synthesized $\text{Fe}_2\text{Mo}_3\text{O}_8$. As shown in Fig. 2(e), the observed diffraction peaks are well indexed to the hexagonal phase of $\text{Fe}_2\text{Mo}_3\text{O}_8$ with the cell parameters of $a = 5.773 \text{ \AA}$, $b = 5.773 \text{ \AA}$, $c = 10.054 \text{ \AA}$, $\alpha = 90.0^\circ$, $\beta = 90.0^\circ$ and $\gamma = 120.0^\circ$ (space group P63mc(186), JCPDS PDF no 36-0526). The corresponding structure of the unit cells is schematically illustrated in Fig. 2(f). In the typical crystal structure of $\text{Fe}_2\text{Mo}_3\text{O}_8$, hybrid octahedral and tetrahedral Fe–O coordinations are connected by octahedral Mo_3 -cluster into a three-dimensional network.

The chemical compositions of the as-synthesized $\text{Fe}_2\text{Mo}_3\text{O}_8$ were also identified via XPS analysis. The XPS survey spectrum in Fig. 3(a) reveals the signals of Fe, Mo, and O. The peaks at 711.4 and 724.7 eV in the high-resolution XPS spectrum of Fe 2p are attributed to $\text{Fe}^{2+} 2p_{3/2}$ and $\text{Fe}^{2+} 2p_{1/2}$, respectively (Fig. 3(b)). Mo 3d core level (Fig. 3(c)) splits into two characteristic doublets. Peaks centered at 234.1 and 230.1 eV correspond to the Mo(IV) $3d_{5/2}$ and $3d_{3/2}$, respectively. Another pair of peaks at 235.7 and 232.4 eV indicate the Mo(VI) state because of the partial surface oxidation during the sample preparation for XPS characterization in air or change in oxygen coordination due to laser degradation process, which is similar to many other $\text{M}_2\text{Mo}_3\text{O}_8$ or molybdenum-based compounds [5,9,30,31]. Figure 3(d) displays the high-resolution XPS spectrum of O 1s. The peak at 530.7 eV can be ascribed to the bonding state of Mo–O or Fe–O. Another peak at 532.1 eV can be attributed to the surface adsorbed moisture [5,10].

To study the porosity and pore structures of $\text{Fe}_2\text{Mo}_3\text{O}_8$ hollow spheres, N_2 adsorption and desorption isotherms were measured on the samples. As shown in Fig. S2 (cf. ESM), the isotherms present the characteristics of type IV isotherm with a certain hysteresis loop appeared at $P/P_0 > 0.4$, indicating that amount of mesopores present in the sample [6]. The resulting sample possesses a BET surface area of $66.5 \text{ m}^2 \cdot \text{g}^{-1}$ with a pore volume of $0.147 \text{ cm}^3 \cdot \text{g}^{-1}$ and an average pore size of ~ 11 nm. This surface area value is much higher than those of $3\text{--}52 \text{ m}^2 \cdot \text{g}^{-1}$ for many other molybdates [6,8,10], which is

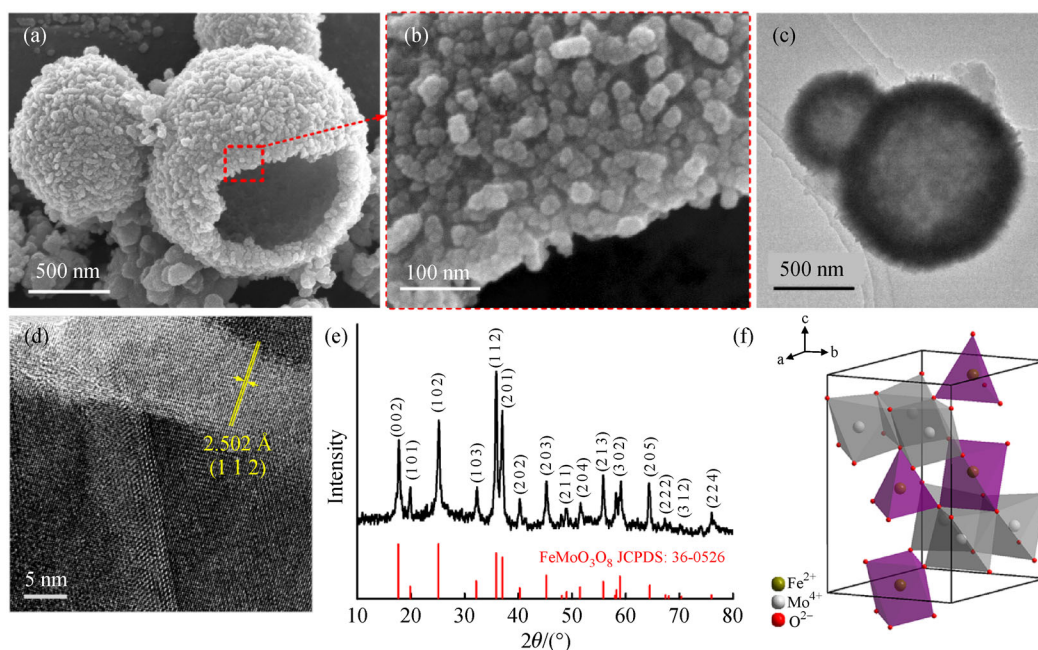


Fig. 2 (a) SEM, (b) locally magnified SEM, (c) TEM, (d) HRTEM images, (e) XRD pattern, and (f) schematic structure of the self-assembled iron(II) molybdenum(IV) oxide ($\text{Fe}_2\text{Mo}_3\text{O}_8$) hollow spheres.

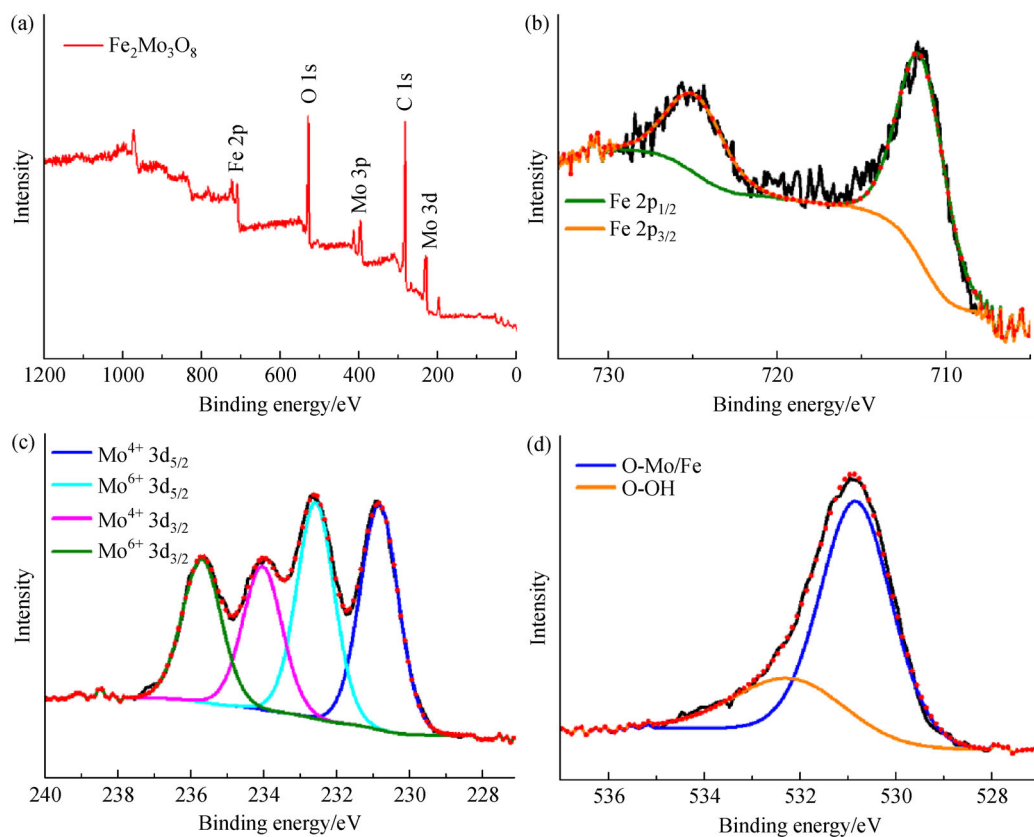


Fig. 3 XPS spectra of the Fe₂Mo₃O₈ hollow spheres: (a) survey spectrum, and high-resolution XPS scan spectra of (b) Fe 2p, (c) Mo 3d and (d) O 1s.

plausibly attributed to the unique hollow sphere structures as well as the self-assembly of nanoparticles that may introduce nanoscale slits or pores on the shells. Such porous structures can accelerate the formation of the electrolyte-electrode interfaces and shorten the transport length for both lithium ions and electrons, which are beneficial for the superior lithium storage [15].

The Li-ion storage properties of the as-synthesized Fe₂Mo₃O₈ hollow spheres were further explored as lithium ion battery anodes. Figure 4(a) displays the CV curves of the initial three cycles in the voltage range of 0.01–3.0 V (vs. Li⁺/Li) at a scan rate of 0.1 mV·s⁻¹. The CV shape is similar with those reported in literature [8,10,32,33]. There is a general sentiment that the initial cathodic peak at ~0.64 V and another large peak at ~0.1 V are attributed to the reduction of Fe²⁺ and Mo⁴⁺ to metallic Fe and Mo, respectively, as well as the formation of solid electrolyte interphase film [8,10,30]. The formation of Mo-metal was confirmed from the *ex situ* TEM characterization when cycled to 0.01 V during 1st cycle (Fig. S3, cf. ESM). Accordingly, the speculated lithium-reaction mechanism is following: Fe₂Mo₃O₈ + 16Li⁺ + 16e⁻ → 2Fe⁰ + 3Mo⁰ + 8Li₂O. Subsequently, the broad anodic peak located in the voltage range of 1.2–1.7 V is attributed to the mixed

oxidation processes of metallic Fe and Mo [5,8,30]. The speculated equations are 2Fe + 2Li₂O ↔ 2FeO + 4Li⁺ + 4e⁻ and 3Mo + 6Li₂O ↔ 3MoO₂ + 12Li⁺ + 12e⁻, respectively, which are consistent with the results in Fe 2p and Mo 3d XPS spectra (Fig. 3). In the following cycles, the decrease in the intensity of the cathodic and anodic peaks is an indication of the capacity fading, which is similar to many previous reports of M₂Mo₃O₈ [5,33,34]. However, the following second and third CV curves are almost identical, indicating that the reaction is stable and reversible.

Figure 4(b) shows the representative discharge-charge curves for the Fe₂Mo₃O₈ hollow spheres at a current density of 100 mA·g⁻¹ with a cutoff potential window of 0.01–3 V vs. Li/Li⁺. The initial discharge and charge capacities are 1189 and 997 mA·h·g⁻¹, respectively, which are higher than the theoretical capacity of 813 mA·h·g⁻¹ based on lithium storage mechanism of redox conversion. The excess capacity of as-prepared Fe₂Mo₃O₈ is probably due to the interfacial charge storage and metallic cluster-like Li storage [35]. The initial irreversible capacity loss of ~16% is generally originated from the formation of solid electrolyte interphase films, as well as the irreversible trapping of lithium ions by the Li₂O lattice [8,9,33].

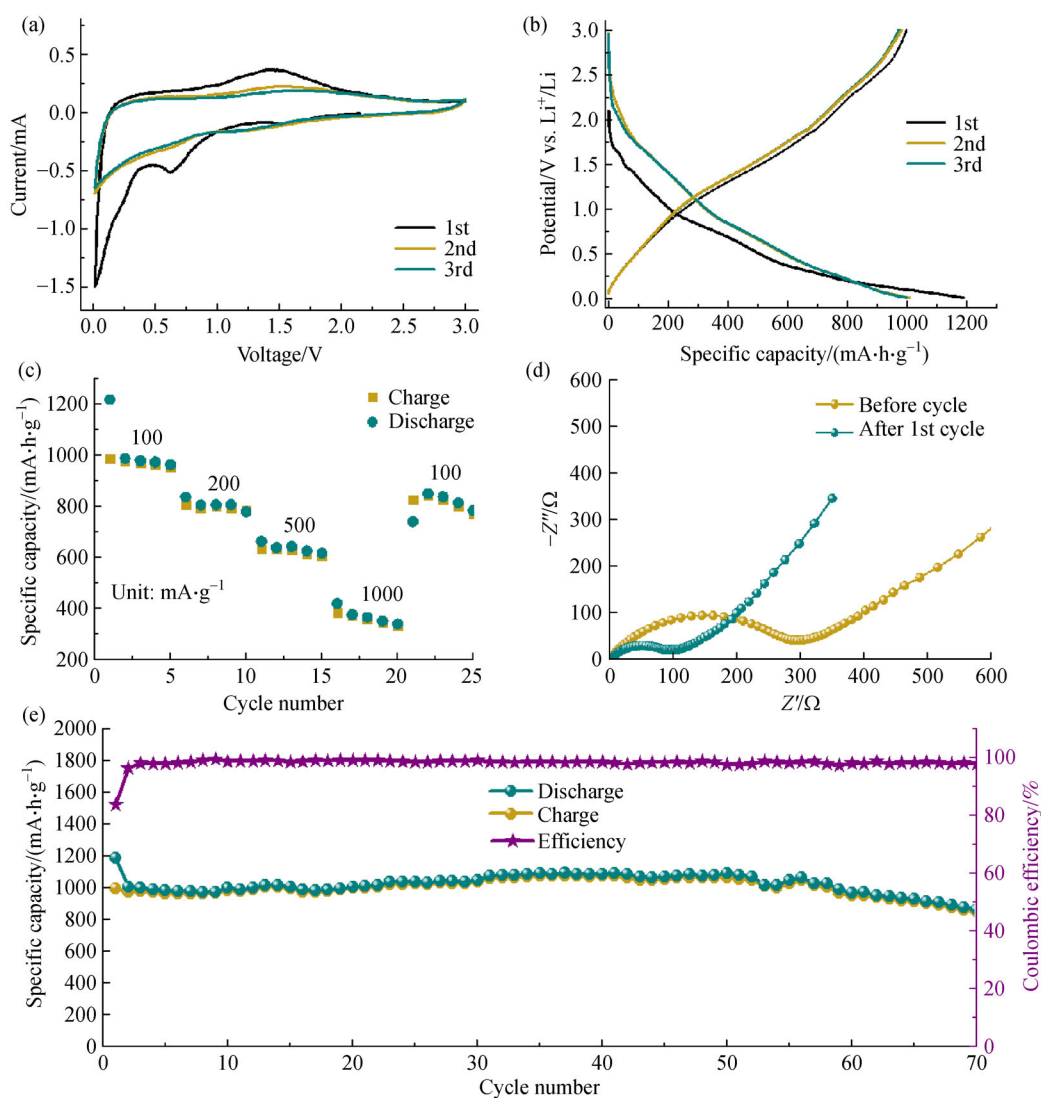


Fig. 4 The electrochemical performances of $\text{Fe}_2\text{Mo}_3\text{O}_8$ hollow spheres: (a) CV curves at $0.1 \text{ mV} \cdot \text{s}^{-1}$; (b) discharge-charge voltage profiles; (c) rate performance; (d) electrochemical impedance spectroscopy (EIS) profiles; (e) cycling performance and Coulombic efficiency of the $\text{Fe}_2\text{Mo}_3\text{O}_8$ electrode.

However, the capacity losses of the second and third cycles are decreasing obviously to $\sim 2.7\%$, suggesting the good reversibility of the $\text{Fe}_2\text{Mo}_3\text{O}_8$ electrode.

To reveal its rate capability, the $\text{Fe}_2\text{Mo}_3\text{O}_8$ electrode was then cycled under various current densities ranging from 0.1 to $1 \text{ A} \cdot \text{g}^{-1}$, as shown in Fig. 4(c). The $\text{Fe}_2\text{Mo}_3\text{O}_8$ electrode can deliver the average discharge capacities of 974 , 806 , 636 , $369 \text{ mA} \cdot \text{h} \cdot \text{g}^{-1}$ at current densities of 0.1 , 0.2 , 0.5 and $1 \text{ A} \cdot \text{g}^{-1}$, respectively. Notably, when the current rate decreases back to $0.1 \text{ A} \cdot \text{g}^{-1}$, a high discharge capacity of $812 \text{ mA} \cdot \text{h} \cdot \text{g}^{-1}$ can still be regained, suggesting the desirable tolerance of the $\text{Fe}_2\text{Mo}_3\text{O}_8$ electrode.

Figure 4(d) presents the EIS of the $\text{Fe}_2\text{Mo}_3\text{O}_8$ electrode before cycle and after the first cycle. The shrinkage of the semi-circles at the high-medium frequencies region is corresponding to the significant decrease of the charge transfer resistance (R_{ct}) after cycling, which is identified by the impedance parameters derived from the equivalent circuit model (Table S1, cf. ESM). Additionally, the Li^+ diffusion coefficient (D_{Li^+}) of $\text{Fe}_2\text{Mo}_3\text{O}_8$ electrode is $1.51 \times 10^{-11} \text{ cm}^2 \cdot \text{s}^{-1}$, which was calculated corresponding to the slope of the linear plot of Z' versus $\omega^{-1/2}$ (Fig. S4, cf. ESM), indicating a relatively sluggish diffusion kinetics that associated with Li^+ diffusion in the bulk electrode

[36–38].

Figure 4(e) shows the repeated discharge–charge cycling performance of the Fe₂Mo₃O₈ electrode at the current densities of 0.1 A·g⁻¹. It is clearly seen that the Fe₂Mo₃O₈ electrode displays an obvious capacity loss in the first cycle, and then remains stable in following cycles. Consequently, a robust capacity retention of 866 mA·h·g⁻¹ is demonstrated over 70 cycles, which retains 87% of the initial reversible capacity. Furthermore, the corresponding Coulombic efficiency values for the whole cycling process stay constant at ~98% after initial several cycles, which further indicates the good stability of the Fe₂Mo₃O₈ electrode.

By comparing the evaluations of our synthesized Fe₂Mo₃O₈ hollow spheres with other M₂Mo₃O₈ molybdates, it is clearly seen that the Fe₂Mo₃O₈ hollow spheres delivery higher or comparable electrochemical properties as Lithium ion batteries anodes (Table S2, cf. ESM). Furthermore, the recently reported Fe₂Mo₃O₈ blocks via solid-state synthesis at 1000 °C and 8 MPa pressure [9] also exhibit much lower reversible capacities of 420 mA·h·g⁻¹ at 50 mA·g⁻¹ than our sample. The enhanced lithium storage properties of the as-synthesized Fe₂Mo₃O₈ in this work can be attributed to the special nanostructure of hollow spheres constructed by fine nanoparticles. These mesoporous hollow spheres can facilitate the electrolyte penetration and simultaneously contact the electrolyte on the inner and outer surfaces of hollow spheres, which not only shortens the diffusion path of lithium ions, but also increases the exposure of effective active sites for Li⁺ insertion/extraction [15].

4 Conclusions

In summary, we utilized the bubble-template-assisted hydrothermal synthetic method combined with a simple calcination to prepare the Fe₂Mo₃O₈ mesoporous hollow spheres with improved lithium ion storage properties. The shells of the hollow spheres have a thickness of about 120 nm on average. They were consisted of small self-assembled Fe₂Mo₃O₈ nanoparticles with the sizes ranging from 10 to 20 nm. Furthermore, the prepared sample possesses a surface area of 66.5 m²·g⁻¹ and an average pore size of ~11 nm. These unique mesoporous hollow spheres can facilitate the electrolyte penetration and provide more active sites for the Li⁺ ions insertion/extraction. When evaluated as a lithium ion battery anode, the proposed Fe₂Mo₃O₈ hollow spheres exhibit highly reversible capacity and good long-term cycling stability. We anticipate that this feasible strategy will lead to new opportunities for the rational design and synthesis in other ternary metal molybdates and tungstates.

Acknowledgements This work was supported by the National Natural Science Foundation of China (Grant Nos. 21203116 and 51602184), the

China Scholarship Council (CSC), the Innovate UK (Grant No. 104013), EPSRC UKRI (EP/T024682/1), the institutional strategic grant-Global Challenges Research Fund (GCRF) that City, University of London receives from Research England, UK Research and Innovation (UKRI), the Natural Science Foundation of Shaanxi (Grant No. 2020JM-502), the funding for platform construction of energy storage materials and devices in Shaanxi University of Science and Technology (Grant No. 0126-126021802).

Electronic Supplementary Material Supplementary material is available in the online version of this article at <https://doi.org/10.1007/s11705-020-1986-x> and is accessible for authorized users.

References

1. Kurumaji T, Takahashi Y, Fujioka J, Masuda R, Shishikura H, Ishiwata S, Tokura Y. Electromagnon resonance in a collinear spin state of a polar antiferromagnet Fe₂Mo₃O₈. *Physical Review B*, 2017, 95(2): 20405–20421
2. Ou H H, Tran Q T P, Lin P H. A synergistic effect between gluconate and molybdate on corrosion inhibition of recirculating cooling water systems. *Corrosion Science*, 2018, 133: 231–239
3. Li Y, Xu H, Huang H, Wang C, Gao L G, Ma T L. One-dimensional MoO₂-Co₂Mo₃O₈@C nanorods: a novel and high efficient oxygen evolution reaction catalyst derived from metal organic framework composite. *Chemical Communications*, 2018, 54(22): 2739–2742
4. Zhang L, Zheng S S, Wang L L, Tang H, Xue H G, Wang G X, Pang H. Fabrication of metal molybdate micro/nanomaterials for electrochemical energy storage. *Small*, 2017, 13(33): 1700917–1700936
5. Gao S S, Tang Y K, Gao Y, Liu Y, Zhao H Y, Li X H, Wang X Z. Highly crystallized Co₂Mo₃O₈ hexagonal nanoplates interconnected by coal-derived carbon via the molten-salt-assisted method for competitive Li-ion battery anodes. *ACS Applied Materials & Interfaces*, 2019, 11(7): 7006–7013
6. Petnikot S, Marka S K, Srikanth V V S S, Reddy M V, Chowdari B V R. Elucidation of few layered graphene-complex metal oxide (A₂Mo₃O₈, A = Co, Mn and Zn) composites as robust anode materials in Li ion batteries. *Electrochimica Acta*, 2015, 178: 699–708
7. Zhang L, He W, Liu Y, Ling M, Zheng P, Guo S. 3D hierarchical flower of copper molybdate Cu₃Mo₂O₉: synthesis, nanostructure and lithium storage properties. *Journal of Alloys and Compounds*, 2017, 723: 512–519
8. Sun Y M, Hu X L, Luo W, Shu J, Huang Y H. Self-assembly of hybrid Fe₂Mo₃O₈-reduced graphene oxide nanosheets with enhanced lithium storage properties. *Journal of Materials Chemistry A, Materials for Energy and Sustainability*, 2013, 1(14): 4468–4474
9. Chu Y Y, Shi X Y, Wang Y, Fang Z Q, Deng Y J, Liu Z X, Dong Q S, Hao Z M. High temperature solid-state synthesis of dopant-free Fe₂Mo₃O₈ for lithium ion batteries. *Inorganic Chemistry Communications*, 2019, 107: 107477–107481
10. Maseed H, Petnikota P, Srikanth V V S S, Srinivasan M, Chowdari B V R, Reddy M V, Adams S. Fe₂Mo₃O₈/exfoliated graphene oxide: solid-state synthesis, characterization and anodic application in Li-ion batteries. *New Journal of Chemistry*, 2018, 42(15): 12817–12823
11. Zhang L, Shen K, He W, Liu Y, Yin L, Guo S. Hierarchical

- nanorods constructed by $\text{Mn}_2\text{Mo}_3\text{O}_8$ @reduced graphene oxide nanosheet arrays with enhanced lithium storage properties. *Journal of Physics and Chemistry of Solids*, 2018, 121: 71–77
- Liang J, Yu X, Zhou H, Wu H B, Ding S J, Lou X W. Bowl-like SnO_2 @carbon hollow particles as an advanced anode material for lithium-ion batteries. *Angewandte Chemie International Edition*, 2014, 53(47): 12803–12807
 - He Y, Zhang Y, Ding F, Li X, Wang Z, Lü Z, Wang X, Liu Z, Huang X. Formation of hollow nanofiber rolls through controllable carbon diffusion for Li metal host. *Carbon*, 2020, 157: 622–630
 - Wang L J, Liu F H, Ning Y S, Bradley R, Yang C B, Yong K, Zhao B Y, Wu W P. Biocompatible mesoporous hollow carbon nanocapsules for high performance supercapacitors. *Scientific Reports*, 2020, 10(1): 4306
 - Lu S J, Wang Z T, Zhang X H, He Z J, Tong H, Li Y J, Zheng J C. *In situ*-formed hollow cobalt sulfide wrapped by reduced graphene oxide as an anode for high-performance lithium-ion batteries. *ACS Applied Materials & Interfaces*, 2020, 12(2): 2671–2678
 - Lu J W, Lan L, Liu X T T, Wang N, Fan X L. Plasmonic Au nanoparticles supported on both sides of TiO_2 hollow spheres for maximising photocatalytic activity under visible light. *Frontiers of Chemical Science and Engineering*, 2019, 13(4): 665–671
 - Liang L W, Sun X, Zhang J Y, Hou L H, Sun J F, Liu Y, Wang S G, Yuan C Z. *In situ* synthesis of hierarchical core double-shell Ti-doped LiMnPO_4 @ $\text{NaTi}_2(\text{PO}_4)_3$ @C/3D graphene cathode with high-rate capability and long cycle life for lithium-ion batteries. *Advanced Energy Materials*, 2019, 9(11): 1802847
 - Liu T F, Zhang Y P, Jiang Z G, Zeng X Q, Ji J P, Li Z H, Gao X H, Sun M H, Lin Z, Ling M, Zheng J, Liang C. Exploring competitive features of stationary sodium ion batteries for electrochemical energy storage. *Energy & Environmental Science*, 2019, 12(5): 1512–1533
 - Zhang L, He W, Ling M, Shen K, Liu Y, Guo S. Cu@MoO_2 @C nanocomposite with stable yolk-shell structure for high performance lithium-ion batteries. *Journal of Alloys and Compounds*, 2018, 768: 714–721
 - Rossetti G A, Burger J L, Sisson R D. Characterization of mixed cobalt-molybdenum oxides prepared by evaporative decomposition of solutions. *Journal of the American Ceramic Society*, 1989, 72(10): 1811–1815
 - Eschenauer H A, Kobelev V V, Schumacher A. Bubble method for topology and shape optimization of structures. *Structural Optimization*, 1994, 8(1): 42–51
 - Nie C, Zeng W, Jing X, Ye H. NiO hollow nanospheres with different surface by a bubble-template approach and its gas sensing. *Journal of Materials Science Materials in Electronics*, 2018, 29(9): 7480–7488
 - Ding C, Yan D, Zhao Y, Zhao Y Z, Zhou H P, Li J B, Jin H B. Bubble-template approach to assemble Ni-Co oxide hollow microspheres with enhanced electrochemical performance as anode for lithium ion batteries. *Physical Chemistry Chemical Physics*, 2016, 18(37): 25879–25886
 - Zuo X X, Chang K, Zhao J, Xie Z Z, Tang H W, Li B, Chang Z R. Bubble-template-assisted synthesis of hollow fullerene-like MoS_2 nanocages as a lithium ion battery anode material. *Journal of Materials Chemistry. A, Materials for Energy and Sustainability*, 2016, 4(1): 51–58
 - Chen R J, Zhao T, Wu W P, Wu F, Li L, Qian J, Xu R, Wu H M, Albishri H M, Al-Bogami A S, El-Hady D A, Lu J, Amine K. Free-standing hierarchically sandwich-type tungsten disulfide nanotubes/graphene anode for lithium-ion batteries. *Nano Letters*, 2014, 14(10): 5899–5904
 - Kozakova Z, Kuritka I, Kazantseva N E, Babayan V, Pastorek M, Machovsky M, Bazant P, Saha P. The formation mechanism of iron oxide nanoparticles within the microwave-assisted solvothermal synthesis and its correlation with the structural and magnetic properties. *Dalton Transactions (Cambridge, England)*, 2015, 44(48): 21099–21108
 - Skrabalak S E, Wiley B J, Kim M, Formo E V, Xia Y N. On the polyol synthesis of silver nanostructures: glycolaldehyde as a reducing agent. *Nano Letters*, 2008, 8(7): 2077–2081
 - Zhou Y, Yao H, Zhang Q, Gong J, Liu S, Yu S. Hierarchical FeWO_4 microcrystals: solvothermal synthesis and their photocatalytic and magnetic properties. *Inorganic Chemistry*, 2009, 48(3): 1082–1090
 - Zhang L, Cao X, Ma Y, Chen X, Xue Z. Microwave-assisted solution-phase preparation and growth mechanism of FeMoO_4 hierarchical hollow spheres. *CrystEngComm*, 2010, 12(1): 207–210
 - Zhang L, Shen K, Li Y, Zha T, Song Y, Liu Y, Guo S. Top-down tailoring of nanostructured manganese molybdate enhances its lithium storage properties. *CrystEngComm*, 2019, 21(36): 5374–5381
 - Tang L B, Zhang B, An C S, Li H, Xiao B, Li J H, He Z J, Zheng J C. Ultrahigh-rate behavior anode materials of MoSe_2 nanosheets anchored on dual-heteroatoms functionalized graphene for sodium-ion batteries. *Inorganic Chemistry*, 2019, 58(12): 8169–8178
 - Das B, Reddy M V, Tripathy S, Chowdari B V R. A disc-like Mo-metal cluster compound, $\text{Co}_2\text{Mo}_3\text{O}_8$, as a high capacity anode for lithium ion batteries. *RSC Advances*, 2014, 4(64): 33883–33889
 - Zhu Y, Zhong Y, Chen G, Deng X, Cai R, Li L, Shao Z. Hierarchical $\text{Zn}_2\text{Mo}_3\text{O}_8$ nanodots-porous carbon composite as a superior anode for lithium-ion batteries. *Chemical Communications*, 2016, 52(60): 9402–9405
 - Das B, Reddy M V, Krishnamoorthi C, Tripathy S, Mahendiran R, Rao G V S, Chowdari B V R. Carbothermal synthesis, spectral and magnetic characterization and Li-cyclability of the Mo-cluster compounds, LiYMo_3O_8 and $\text{Mn}_2\text{Mo}_3\text{O}_8$. *Electrochimica Acta*, 2009, 54(12): 3360–3373
 - Kim H, Choi W, Yoon J, Um J H, Lee W, Kim J, Cabana J, Yoon W S. Exploring anomalous charge storage in anode materials for next generation Li rechargeable batteries. *Chemical Reviews*, 2020, 120(14): 6934–6976
 - Zheng J C, Yang Z, He Z J, Tong H, Yu W J, Zhang J F. *In situ* formed $\text{LiNi}_{0.8}\text{Co}_{0.15}\text{Al}_{0.05}\text{O}_2$ @ Li_4SiO_4 composite cathode material with high rate capability and long cycling stability for lithium-ion batteries. *Nano Energy*, 2018, 53: 613–621
 - Xiao B, Zhang W, Wang P, Tang L B, An C, He Z, Tong H, Zheng J, Wang B. An C S, He Z J, Tong H, Zheng J C, Wang B. $\text{V}_2(\text{PO}_4)_3$ encapsulated into crumpled nitrogen-doped graphene as a high-

- performance anode material for sodium-ion batteries. *Electrochimica Acta*, 2019, 306: 238–244
38. Zuo D H, Song S C, An C S, Tang L B, He Z J, Zheng Z C. Synthesis of sandwich-like structured Sn/SnO_x@MXene composite through *in-situ* growth for highly reversible lithium storage. *Nano Energy*, 2019, 62: 401–409